BIOCHEMISTRY
including biophysical chemistry & molecular biology
Article

Biochemistry **2010,** *49,* 7683–7693 7683
DOI: 10.1021/bi100458d

Structural Insight into Methyl-Coenzyme M Reductase Chemistry Using Coenzyme B Analogues[†,‡]

Peder E. Cedervall,[§,#] Mishtu Dey,[∥,#,⊥] Arwen R. Pearson,[§,△] Stephen W. Ragsdale,[∥] and Carrie M. Wilmot*[,§]

[§]*Department of Biochemistry, Molecular Biology, and Biophysics, University of Minnesota, Minneapolis, Minnesota 55455, and* [∥]*Department of Biological Chemistry, University of Michigan, Ann Arbor, Michigan 48109.* [#]*These authors contributed equally to this work.* [⊥]*Current address: Department of Chemistry, Massachusetts Institute of Technology, 77 Massachusetts Ave., Cambridge, MA 02139.* [△]*Current address: Astbury Centre for Structural Molecular Biology, Institute for Molecular and Cellular Biology, Astbury Building, Leeds LS2 9JT, U.K.*

Received March 27, 2010; Revised Manuscript Received July 21, 2010

ABSTRACT: Methyl-coenzyme M reductase (MCR) catalyzes the final and rate-limiting step in methane biogenesis: the reduction of methyl-coenzyme M (methyl-SCoM) by coenzyme B (CoBSH) to methane and a heterodisulfide (CoBS-SCoM). Crystallographic studies show that the active site is deeply buried within the enzyme and contains a highly reduced nickel-tetrapyrrole, coenzyme F_{430}. Methyl-SCoM must enter the active site prior to CoBSH, as species derived from methyl-SCoM are always observed bound to the F_{430} nickel in the deepest part of the 30 Å long substrate channel that leads from the protein surface to the active site. The seven-carbon mercaptoalkanoyl chain of CoBSH binds within a 16 Å predominantly hydrophobic part of the channel close to F_{430}, with the CoBSH thiolate lying closest to the nickel at a distance of 8.8 Å. It has previously been suggested that binding of CoBSH initiates catalysis by inducing a conformational change that moves methyl-SCoM closer to the nickel promoting cleavage of the C−S bond of methyl-SCoM. In order to better understand the structural role of CoBSH early in the MCR mechanism, we have determined crystal structures of MCR in complex with four different CoBSH analogues: pentanoyl, hexanoyl, octanoyl, and nonanoyl derivatives of CoBSH (CoB_5SH, CoB_6SH, CoB_8SH, and CoB_9SH, respectively). The data presented here reveal that the shorter CoB_5SH mercaptoalkanoyl chain overlays with that of CoBSH but terminates two units short of the CoBSH thiolate position. In contrast, the mercaptoalkanoyl chain of CoB_6SH adopts a different conformation, such that its thiolate is coincident with the position of the CoBSH thiolate. This is consistent with the observation that CoB_6SH is a slow substrate. A labile water in the substrate channel was found to be a sensitive indicator for the presence of CoBSH and HSCoM. The longer CoB_8SH and CoB_9SH analogues can be accommodated in the active site through exclusion of this water. These analogues react with Ni(III)-methyl, a proposed MCR catalytic intermediate of methanogenesis. The CoB_8SH thiolate is 2.6 Å closer to the nickel than that of CoBSH, but the additional carbon of CoB_9SH only decreases the nickel thiolate distance a further 0.3 Å. Although the analogues do not induce any structural changes in the substrate channel, the thiolates appear to preferentially bind at two distinct positions in the channel, one being the previously observed CoBSH thiolate position and the other being at a hydrophobic annulus of residues that lines the channel proximal to the nickel.

Methanogenic archaea are organisms that under strict anaerobic conditions derive energy by reducing compounds such as carbon dioxide, methylamine, acetate, and methanol to methane (*1*, *2*). The global production of methane by these organisms is estimated at one billion tons annually. Microbially produced methane is not only a potential source of renewable energy but also a potent greenhouse gas, and as such study of this process has environmental ramifications. In these microorganisms, methyl-coenzyme M reductase (MCR)[1] is the enzyme that catalyzes the final step in methanogenesis, in which the substrates methyl-coenzyme M (methyl-SCoM, 2-(methylthio)ethanesulfonate) and coenzyme B (CoBSH, *N*-7-mercaptoheptanoylthreonine phosphate) are converted to methane and a heterodisulfide (CoBS-SCoM) (Scheme 1) (*3*).

MCR is a 272 kDa protein with six subunits arranged in an $\alpha_2\beta_2\gamma_2$ oligomer (*4*). The known crystal structures show that MCR has two active sites approximately 50 Å apart that are deeply buried within the enzyme (*5*). The active site pocket is comprised of residues from subunits α, α′, β, and γ, with a 30 Å long substrate channel leading to the enzyme surface (Figure 1). At the heart of the active site pocket is coenzyme F_{430}, which is a highly reduced nickel-containing tetrapyrrole (*6*−*8*). Currently, 16 distinct enzymatic and complexed states of MCR have been spectroscopically characterized (Supporting Information, Scheme S1) (*9*−*31*).

[†]This work was supported by Department of Energy Grant DE-FG02-08ER15931 to S.W.R. and supplement to C.M.W. and Minnesota Partnership for Biotechnology and Medical Genomics Grant SPAP-05-0013-P-FY06.

[‡]Coordinates and structure factors have been deposited in the Protein Data Bank as entries 3m1v (MCR_{HSCoM}), 3m2r (MCR_{CoB5SH}), 3m2u (MCR_{CoB6SH}), 3m2v (MCR_{CoB8SH}), and 3m30 (MCR_{CoB9SH}).

*Address correspondence to this author. Tel: (612) 624-2406. Fax: (612) 624-5121. E-mail: wilmo004@umn.edu.

[1]Abbreviations: MCR, methyl-coenzyme M reductase; methyl-SCoM, methyl-coenzyme M; CoBSH, coenzyme B; HSCoM, coenzyme M; CoBS-SCoM, heterodisulfide of coenzyme B and coenzyme M; APS, Advanced Photon Source; ASU, asymmetric unit; BPS, bromopropanesulfonate.

Published on Web 07/22/2010

In the resting active state of the enzyme, denoted MCR_{red1}, the redox-active nickel of F_{430} is present in the Ni(I) state (*9*, *16*, *32*). MCR is extremely oxygen sensitive, and upon oxygen exposure the enzyme enters an inactive Ni(II) state, denoted $MCR_{red1\text{-}silent}$ (*6*). In this state it cannot be converted back to the active Ni(I) form by any known reducing agent, making this a challenging system to study. Additional complications involve the tight association of coenzymes to purified MCR that are not easily displaced as demonstrated by X-ray crystallographic and kinetic studies (*5*, *33*−*35*).

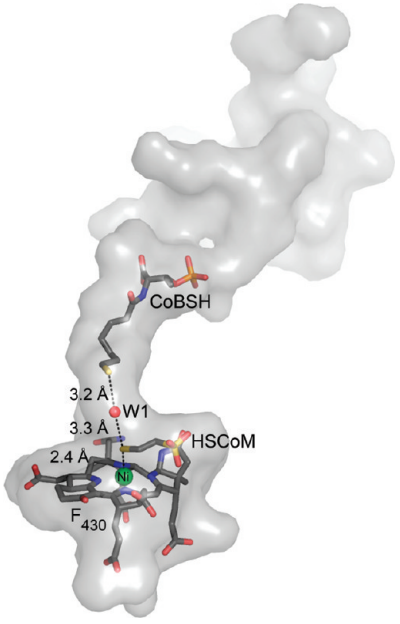

FIGURE 1: The active site and substrate channel in the $MCR_{ox1\text{-}silent}$ crystal structure (PDB code 1hbn) (*9*). Coenzyme F_{430}, CoBSH, and HSCoM are drawn as stick colored by atom (carbon: dark gray). The nickel is displayed as a green sphere and water as a red sphere. Interactions are drawn as dashed lines, and the corresponding distance is indicated in angstroms (Å). The path of the substrate channel was defined in the absence of F_{430}, CoBSH, HSCoM, and water, with the surface closest to the viewer cut away. The figure was generated using PyMOL (http://www.pymol.org).

Scheme 1: Reaction Catalyzed by Methyl-Coenzyme M Reductase

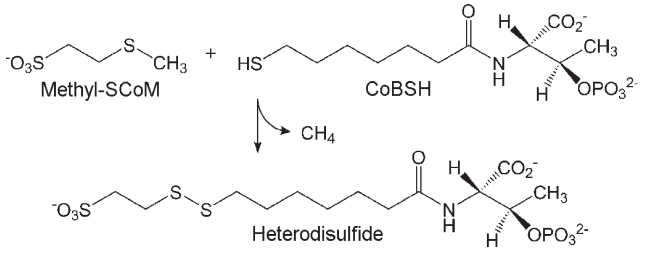

Despite the fact that MCR has been studied for decades, no true catalytic intermediate has been observed, and the actual mechanism remains elusive. Currently, three general mechanistic schemes for the enzymatic reaction have been proposed, each of which posit different chemistry to initiate catalysis. Mechanism I involves Ni(I) acting as a nucleophile in an S_N2-type reaction that generates Ni(III)-methyl as an intermediate (Scheme 2A) (*35*−*38*). Mechanism II starts with methyl-SCoM undergoing homolytic cleavage at the Ni(I) to generate a methyl radical and a Ni(II)-SCoM species (Scheme 2B) (*39*−*41*). A more recently proposed mechanism III suggests protonation of coenzyme F_{430} promotes reductive cleavage of the methyl-SCoM thioether bond (*42*).

Due to the stringent requirement to exclude O_2, the available MCR crystal structures are all in the inactive Ni(II) state. All but one contain CoBSH and HSCoM (demethylated methyl-SCoM, an inhibitor and substrate analogue) in the active site (PDB codes 1hbn, 1hbo, 1hbu, 1e6y, and 1e6v) (*5*, *33*, *34*). Another crystal structure has bound heterodisulfide product, CoBS-SCoM (MCR_{silent}, PDB code 1hbm, Scheme 1 and Supporting Information, Scheme S1) (*5*, *33*). All of these structures reveal that both substrates access the active site through the same channel (Figure 1). The binding site of HSCoM (and presumably methyl-SCoM) is more deeply buried within the enzyme, and so it must enter prior to CoBSH for productive chemistry to occur. As binding of CoBSH in the absence of cosubstrate would be inhibitory, it was suggested that a conformational change upon methyl-SCoM binding might lower the K_d for CoBSH and thus promote an ordered mechanism. Furthermore, it has been suggested that CoBSH binding induces a conformational change that brings the methyl-SCoM substrate into closer proximity to the nickel, and this promotes C−S bond cleavage. To investigate the proposed structural role of CoBSH in initiating catalysis, we have solved the X-ray crystal structures of MCR in complex with four different CoBSH analogues. CoBSH has a heptanoyl moiety linked to the thiol group, and the analogues are pentanoyl-, hexanoyl-, octanoyl-, or nonanoyl-containing derivatives of CoBSH (CoB_5SH, CoB_6SH, CoB_8SH, and CoB_9SH, respectively; Figure 2) (*3*, *35*, *43*−*47*). In addition, we present a structure in which the substrate channel predominantly lacks either CoBSH or heterodisulfide product.

Scheme 2: Two of the Proposed Catalytic Mechanisms for Methyl-Coenzyme M Reductase: (A) Mechanism I; (B) Mechanism II

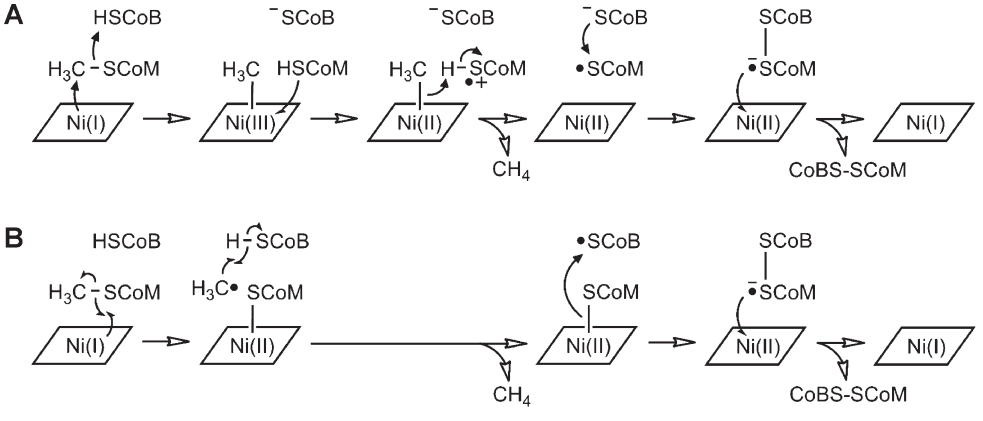

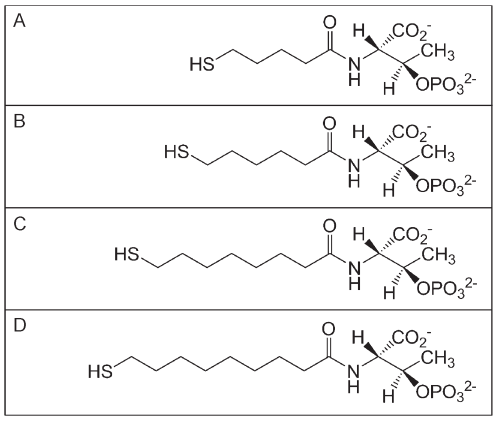

FIGURE 2: Drawing of CoBSH analogues: (A) *N*-5-mercaptopentanoylthreonine phosphate (CoB_5SH); (B) *N*-6-mercaptohexanoylthreonine phosphate (CoB_6SH); (C) *N*-8-mercaptooctanoylthreonine phosphate (CoB_8SH); (D) *N*-9-mercaptononanoylthreonine phosphate (CoB_9SH).

MATERIALS AND METHODS

Materials. The organism *Methanothemobacter marburgensis* (catalog OCM82) was obtained from the Oregon Collection of Methanogens (Portland, OR). All buffers and media reagents were obtained from Sigma-Aldrich (St. Louis, MO). The gases N_2 (99.98%), H_2/CO_2 (80%/20%), and ultra high purity H_2 (99.999%) were obtained from Cryogenic Gases (Grand Rapids, MI). Titanium(III) citrate solutions were prepared from a stock solution of 246 mM titanium(III) citrate, which was synthesized by adding sodium citrate to titanium(III) trichloride (30 wt % solution in 2 N hydrochloric acid) (Acros Organics, Morris Plains, NJ) under anaerobic conditions and adjusting pH to 7.0 with sodium bicarbonate (*48*). The concentration of titanium(III) citrate was determined by titrating against a solution of methyl viologen.

Synthesis of Methyl-SCoM, CoB_5SH, CoB_6SH, CoBSH, CoB_8SH, and CoB_9SH. Methyl-SCoM was prepared from HSCoM and methyl iodide (*49*). The homodisulfides CoB_5S-$SCoB_5$, CoB_6S-$SCoB_6$, CoBS-SCoB, CoB_8S-$SCoB_8$, and CoB_9S-$SCoB_9$ were prepared as described from 5-bromovaleric acid, 6-bromohexanoic acid (Sigma-Aldrich, St. Louis, MO), 7-bromoheptanoic acid (Karl Industries, Aurora, OH), 8-bromooctanoic acid, and 9-bromononanoic acid (Matrix Scientific, Columbia, SC), respectively (*43*, *46*). The free thiol forms of CoB_5SH, CoB_6SH, CoBSH, CoB_8SH, and CoB_9SH were generated by the reduction of the homodisulfides as previously described (*45*). The purity of the CoBSH analogues was determined by ^1H NMR spectroscopy. All compounds synthesized were stored in a Vacuum Atmospheres chamber maintained at an oxygen level below 1 ppm, as monitored continually with an oxygen analyzer (model 317; Teledyne Analytical Instruments, City of Industry, CA) until use.

M. marburgensis Growth and MCR_{red1} Purification. Buffer preparations and all manipulations were performed under strict anaerobic conditions in a Vacuum Atmospheres chamber maintained at an oxygen level below 1 ppm, as monitored continually with an oxygen analyzer (model 317; Teledyne Analytical Instruments, City of Industry, CA). MCR_{red1} was isolated from *M. marburgensis* cultured on H_2/CO_2 (80%/20%) at 65 °C in a 14 L fermentor (New Brunswick Scientific Co., Inc., New Brunswick, NJ). Culture media were prepared as previously described (*20*, *24*). MCR_{red1} was generated *in vivo* and purified as described previously (*20*). The purification procedure routinely generates 65−75% MCR_{red1} as determined by UV−visible and EPR spectroscopy.

Spectroscopy of MCR. UV−visible spectra of the Ni(I)-containing MCR_{red1} were recorded in the anaerobic chamber using a spectrophotometer (model USB4000-UV−vis; Ocean Optics, Dunedin, FL). EPR spectra were recorded on a Bruker EMX spectrometer (Bruker Biospin Corp., Billerica, MA), equipped with an Oxford ITC4 temperature controller, a Hewlett-Packard Model 5340 automatic frequency counter, and Bruker gaussmeter. The EPR spectroscopic parameters included the following: temperature, 70 K; microwave power, 10 mW; microwave frequency, 9.43 GHz; receiver gain, 2×10^4; modulation amplitude, 10.0 G; modulation frequency, 100 kHz. Double integrations of the EPR spectra were performed and referenced to a 1 mM copper perchlorate standard. The NMR data were acquired at 298 K on a Bruker Avance DRX 500 MHz instrument equipped with a TXI cryoprobe.

Preparation of MCR_{red1} for Crystallization. All crystallization experiments were performed in the anaerobic chamber in which MCR was purified unless otherwise noted. MCR_{red1} was prepared in 50 mM Tris, pH 7.6, and excess HSCoM was removed by buffer exchange using an Amicon Ultra centrifuge filter with a 50 kDa cutoff membrane (Millipore). Typically, 2−3 mL of MCR_{red1} was exchanged with 10−15 mL of 50 mM Tris, pH 7.6. The enzyme was concentrated to 500−600 μL, and this process was repeated three times. The fraction of MCR_{red1} in the purified MCR sample was calculated from the UV−visible spectrum using extinction coefficients of 27.0 mM^{-1} cm^{-1} at 385 nm for Ni(I)-MCR_{red1} and 9.15 mM^{-1} cm^{-1} at 420 nm for Ni(II)-$MCR_{red1\text{-}silent}$ (*20*). The amount of MCR_{red1} in samples used for crystallization was determined to be ~80%, and the concentration of total enzyme used was in the range of about 120−150 μM (~32−40 mg/mL). All crystallization experiments were performed anaerobically by incubating 2.0 μL of enzyme solution in 50 mM Tris, pH 7.5, and 2.0 μL of reservoir solution (100 mM Hepes-Na, pH 7.3/7.5/8.0; 150 mM magnesium acetate ($Mg(CH_3COO)_2$), and 20/22% (w/v) PEG 400) in a sitting drop over 1 mL of reservoir solution at 9 °C. Triangular and rectangular prismatic crystals with a bright yellowish green color confirmed the presence of nickel coenzyme F_{430}. The crystals grew to a size of approximately 100−200 μm in 4−5 days. CoBSH-depleted crystals were obtained by incubating 2 μL of a reaction mixture containing 139 μM MCR_{red1} and 13 mM HSCoM with 2 μL of reservoir solution (100 mM Hepes-Na, pH 7.5, 150 mM magnesium acetate ($Mg(CH_3COO)_2$), 22% PEG 400). Crystals of MCR complexed with the CoBSH analogues were grown by cocrystallization. The CoB_5SH cocrystals were obtained by incubating 2 μL of enzyme solution containing 124 μM MCR_{red1}, 10 mM methyl-SCoM, and 1 mM CoB_5SH with 2 μL of reservoir solution (100 mM Hepes-Na, pH 7.5, 150 mM ($Mg(CH_3COO)_2$), 22% PEG 400). The crystals with bound CoB_6SH and CoB_9SH were obtained by cocrystallization of 1 mM analogue with 142 μM MCR_{red1} and equilibrated with 2 μL of reservoir solution (100 mM Hepes-Na, pH 7.5, 150 mM $Mg(CH_3COO)_2$, 20% PEG 400 for CoB_6SH and 100 mM Hepes-Na, pH 7.3, 150 mM $Mg(CH_3COO)_2$), 22% PEG 400 for CoB_9SH). Crystals were cryoprotected in reservoir solution containing 25% (v/v) PEG 400 by soaking for 2−5 min before cryocooling in liquid nitrogen in the anaerobic chamber. Crystals of CoB_8SH bound to MCR were obtained by incubating 2 μL of a mixture of 119 μM MCR_{red1} and 1 mM CoB_8SH with 2 μL of reservoir solution (100 mM Hepes-Na, pH 7.3, 150 mM

$Mg(CH_3COO)_2$), 20% PEG 400). Before cryoprotection, the crystals were soaked for 5−10 min in a 100 mM solution of methyl iodide.[2] The methyl iodide solution used for soaking was prepared by adding a concentrated stock of methanolic solution of methyl iodide to the reservoir solution. Soaked crystals were quickly cryoprotected as described above and cryocooled in the anaerobic chamber.

X-ray Diffraction Data Collection, Processing, and Refinement. X-ray diffraction data were collected at 100 K on a ADSC Quantum-315 detector at the APS Beamline 14-BM-C (BioCARS). The wavelength of X-rays was 0.979 Å. Data were processed using HKL2000 (*50*). As in the previous X-ray crystallographic studies, the crystals belong to the monoclinic space group $P2_1$ (a = 82 Å, b = 118 Å, c = 122 Å, β = 92°), with one MCR molecule (two active sites) per asymmetric unit (*5*, *33*). For refinement, REFMAC in the Collaborative Computational Project Number 4 (CCP4) program suite was used (*51*). A random sample of 5% of the data across all resolution shells was chosen to check refinement progress through calculation of an R_{free}. The same reflections were used to calculate R_{free} for all structures, thus preventing bias due to high structural identity. The remaining reflections were used in refinement (R_{work}). Model building was done using the Crystallographic Object-Oriented Toolkit (COOT) (*52*). The diffraction data and their models are designated as MCR_{CoBXSH}, where X is the number of carbons in the alkanoyl portion of the analogue. Library files in CCP4 for F_{430} and CoBSH were incorrect, and these were modified in Monomer Library Sketcher in the CCP4 program suite by comparison with schematic drawings from Grabarse et al. (*33*). Coordinate and CCP4 library files for the different CoBSH analogues were created in Monomer Library Sketcher. The general model building and refinement strategy for all structures was as follows. It was clear from the electron density in the substrate channel and at the active site that mixtures of species were present in all data sets. These could be visualized with $F_o - F_c$ and $F_o - F_o$ difference electron density maps (Supporting Information, Figure S1). The known positions of CoBSH and HSCoM from the published Ni(II)-MCR crystal structures (PDB codes 1hbn, 1hbo, 1hbu (*33*)) were used as guides to determine which species could be present in each data set, and these were then simultaneously modeled into the electron density. By alteration of their relative occupancies (in 10% increments) followed by refinement, the ratio of occupancy between different species was determined using the assumption that the average *B*-factors for all molecular species bound should be similar to that of F_{430} and adjacent well-ordered protein atoms within the active site and substrate channel. The combinations of modeled ligands were constantly reassessed throughout refinement based on the remaining difference electron density. This included test refinements of different ligand combinations during the latter stages, thus using the optimized phases to check whether a different combination of ligands could also explain the electron density. Sensible chemical structures and interactions, along with keeping the combined occupancies of sterically mutually exclusive species ≤100%, were maintained throughout refinement. The model was finally accepted when the difference electron density map was minimal and the *B*-factors for the models converged.

[2]Methyl iodide was added with the intention of creating a Ni(III)-methyl species. This was not achieved, but the diffraction quality of this crystal was significantly better than crystals cocrystallized with CoB_8SH alone and so has been included in this study.

The first structure refined was that of MCR_{CoB5SH}. Initial phases were generated by difference Fourier using a previously determined crystal structure (PDB code 1mro (*5*)) but with all nonbonded molecules, including water, removed from the model except F_{430}. Initial rigid body refinement followed by restrained refinement of MCR_{CoB5SH} reduced the R_{work} to 26.5%. After model building and subsequent rounds of restrained refinement the R_{work} was 14.3% (R_{free} 16.6%). Of the five structures only the CoB_5SH analogue is completely coincident with CoBSH, and so particular care had to be used in teasing apart the ratios of the two species in modeling the MCR_{CoB5SH} electron density. This was done by initially refining 100% CoBSH in the substrate channel. Positive $F_o - F_c$ difference density located at the carbon where the shorter CoB_5SH thiol might be expected to be indicated the presence of a more electron-rich species than carbon, which is consistent with the presence of the CoB_5SH sulfur. The refinement converged at a model containing a 50:50 mix of CoBSH and the analogue. However, positive $F_o - F_c$ difference density was still present at the position of the CoBSH thiol; therefore, a water molecule was added to the CoB_5SH model at 50% occupancy, and upon refinement this accounted for the electron density. An illustration of the electron density quality from this structure is shown in Supporting Information, Figure S2. An HSCoM-, CoBSH-, and CoBSH analogue-free version of the refined MCR_{CoB5SH} structure was used as the starting model to generate initial phases for the four other structures. After the initial round of restrained refinement the R_{work} for these structures were reduced to 14.5−15.6%.

RESULTS AND DISCUSSION

Crystal Structures of MCR. Five crystal structures were determined, four of which are in complex with CoBSH analogues differing in the number of carbons atoms in the alkanoyl portion of the molecule. CoBSH is an *N*-7-mercaptoheptanoyl-containing molecule, whereas the four CoBSH analogues contain *N*-5-mercaptopentanoyl, *N*-6-mercaptohexanoyl, *N*-8-mercaptooctanoyl, or *N*-9-mercaptononanoyl moieties (Figure 2). The corresponding crystal structures are designated as MCR_{CoBXSH}, where X is the number of carbons in the alkanoyl portion of the analogue. The other crystal structure is of $MCR_{red1c\text{-}silent}$ (MCR in the Ni(II) state in complex with HSCoM, designated here as MCR_{HSCoM}) that is CoBSH-depleted. The data sets have resolutions from 1.3 to 1.8 Å. Although the crystallizations were set up with the MCR solution predominantly in the Ni(I)-MCR_{red1} state, by the time X-ray diffraction data were collected the crystals had been oxidized to the Ni(II)-$MCR_{red1\text{-}silent}$ state (Supporting Information). Following data collection there was no evidence for photoreduction of the Ni(II) back to Ni(I) in any of the crystals, as assessed by single crystal UV−visible microspectrophotometry (Supporting Information and Figure S3). Attempts to photoreduce the crystals using different wavelengths and temperatures were unsuccessful (Supporting Information).

Overall, the resulting structures are very similar to each other and to the previously published structures of MCR, with differences mainly localized to the active site and substrate channel. The two active sites in the ASU were refined independently. Unless otherwise stated, there was no difference between them. All five data sets contain a mixture of species bound to the enzyme. There is always a background of CoBSH and HSCoM, which copurify with MCR and cannot be fully removed by extensive buffer exchange or by the addition of a CoBSH

Table 1: X-ray Data Collection, Processing, and Refinement Statistics

data collection and processing statistics					
name of data set	MCR_{CoB5SH}	MCR_{CoB6SH}	MCR_{HSCoM}	MCR_{CoB8SH}	MCR_{CoB9SH}
measured reflections	1969388	2427498	1440665	1160543	1425506
unique reflections	553755	446253	405349	211803	401701
resolution (Å)[a]	50.0−1.30 (1.35−1.30)	50.0−1.40 (1.45−1.40)	50.0−1.45 (1.50−1.45)	50.0−1.80 (1.86−1.80)	50.0−1.45 (1.50−1.45)
completeness (%)[a]	97.1 (78.1)	99.9 (100.0)	99.5 (99.7)	99.8 (100.0)	98.1 (95.4)
R-sym (%)[a,b]	5.5 (32.9)	7.3 (44.7)	6.2 (44.0)	8.4 (47.7)	5.6 (42.5)
$I/\sigma I$[a]	22.3 (3.6)	20.4 (4.0)	20.2 (3.2)	21.8 (3.9)	24.3 (3.2)
space group	$P2_1$	$P2_1$	$P2_1$	$P2_1$	$P2_1$
refinement and model building statistics					
resolution (Å)[a]	20.49−1.30 (1.33−1.30)	19.89−1.40 (1.44−1.40)	20.15−1.45 (1.49−1.45)	19.93−1.80 (1.84−1.80)	20.07−1.45 (1.48−1.45)
no. of reflections in working set[a]	525817 (30239)	423854 (25833)	384868 (25791)	201128 (11193)	381474 (23611)
no. of reflections in test set[a]	27777 (1576)	22348 (1331)	20362 (1319)	10625 (557)	20163 (1210)
R-work (%)[c]	14.32	13.04	13.47	14.95	13.58
R-free (%)[d]	16.56	15.53	16.22	19.54	16.44
ESU (Å) *R*-work/*R*-free	0.044/0.046	0.049/0.051	0.056/0.059	0.121/0.119	0.057/0.060
no. of protein atoms	20087	19960	20265	19750	20036
no. of coenzyme atoms	218	220	180	224	272
no. of ligand atoms	37	62	52	26	49
no. of water molecules	2443	2352	2516	1893	2432
rms					
bond lengths (Å)	0.033	0.033	0.032	0.028	0.032
bond angles (deg)	2.693	2.625	2.468	2.059	2.549
Ramachandran plot (%)					
favored	97.8	97.5	97.6	97.2	97.7
allowed	2.1	2.4	2.3	2.7	2.1
disallowed	0.1	0.1	0.1	0.1	0.1
average *B*-factor (Å^2)					
protein	12.42	13.35	12.12	17.22	12.73
coenzymes	8.20	9.24	7.25	11.24	8.27
ligands	31.95	35.48	28.29	33.76	32.92
waters	22.95	24.89	23.85	26.79	24.09
over all	13.54	14.57	13.40	18.02	13.93
occupancy of HSCoM per active site (%)[e]	90/90	50/50	100/100	90/90	90/85
occupancy of CoBSH per active site (%)[e]	50/50	50/50	30/30	50/50	40/40
CoBSH analogue, occupancy per active site (%)[e]	CoB_5SH, 50/50	CoB_6SH, 50/50		CoB_8SH, 50/50	CoB_9SH, 60/60
other molecule, occupancy per active site (%)[e]			acetate, 70/70		

[a]Values in parentheses correspond to the highest resolution shell. [b]*R*-sym = $\sum_{hkl}\sum_{j=1}^{N}|I_{hkl} - I_{hkl}(j)|/\sum_{hkl}NI_{hkl}$, sum over all reflections and all observations *N*, with $I_{hkl}(j)$ intensity of the *j*th observation of reflection *hkl* and I_{hkl} mean intensity of the reflection *hkl*. [c]*R*-work = $\sum||F_o| - |F_c||/\sum|F_o|$, where $|F_o|$ = observed structure factor amplitude and $|F_c|$ = calculated structure factor amplitude. [d]*R*-free, *R*-factor based on 5% of the data excluded from refinement. [e]Occupancy of model in each of the two crystallographically independent active sites in the ASU.

analogue. HSCoM is added during purification of MCR, as it stabilizes the resting active Ni(I) state (unpublished data), and this leads to HSCoM occupancies between 50% and 100% among the structures (Table 1). In contrast, CoBSH, which is not added during purification, has occupancies ranging from 30% to 50%. As these confounding species have all been described at high occupancy in other crystallographic studies, the structural data of interest could be isolated (*5*, *33*). In each case, the additional electron density could be explained by inclusion of the appropriate CoB_XSH model used in that experiment at 50% or higher occupancy. The resulting models, along with $2F_o - F_c$ electron density, are shown in Figure 3. The R_{work} for the final structures range from 13.0% to 15.0% (R_{free} 15.5−19.5%). The X-ray data collection, processing, refinement, and model building statistics are given in Table 1.

Analogues Shorter Than CoBSH: CoB_5SH and CoB_6SH. CoB_5SH is two methylene groups shorter than CoBSH, the MCR substrate. The MCR_{CoB5SH} structure is to 1.3 Å resolution. As expected, the pentanoyl chain follows the path of the CoBSH heptanoyl carbons down the substrate channel, and thus its thiol is positioned in the same place as the second carbon preceding the CoBSH thiol (Figures 3A and 4). There are no published MCR kinetic studies using CoB_5SH, but as it binds in the substrate channel, it is likely to be an inhibitor.

CoB_6SH is one methylene shorter than CoBSH and is a slow substrate of MCR. In this case the 1.4 Å resolution electron density of MCR_{CoB6SH} indicates that the analogue unexpectedly binds in the substrate channel such that its thiol is virtually in the same position as the thiol of CoBSH (Figures 3B and 4). The hexanoyl chain is oriented so that it takes a shorter route down the substrate channel between carbons 2 and 5 (with the carbonyl carbon labeled as carbon 1) than CoBSH (Figure 4, Supporting Information, Figure S4). This shortcut is not seen in any of the other CoB_XSH complex crystal structures but presumably arises because this CoB_6SH binding conformer is energetically more favorable, although it is not clear from the structure why this might be the case. CoB_6SH binds very tightly to MCR, with an apparent K_i value of 0.1 μM (*3*).

Water Structure in the Absence of HSCoM. The electron density for the MCR_{CoB6SH} crystal structure only supported the modeling of 50% bound HSCoM. In the fraction of MCR molecules where HSCoM is absent, the HSCoM binding site is occupied by a network of four water molecules (Supporting Information, Figure S5). Two waters are positioned close to the

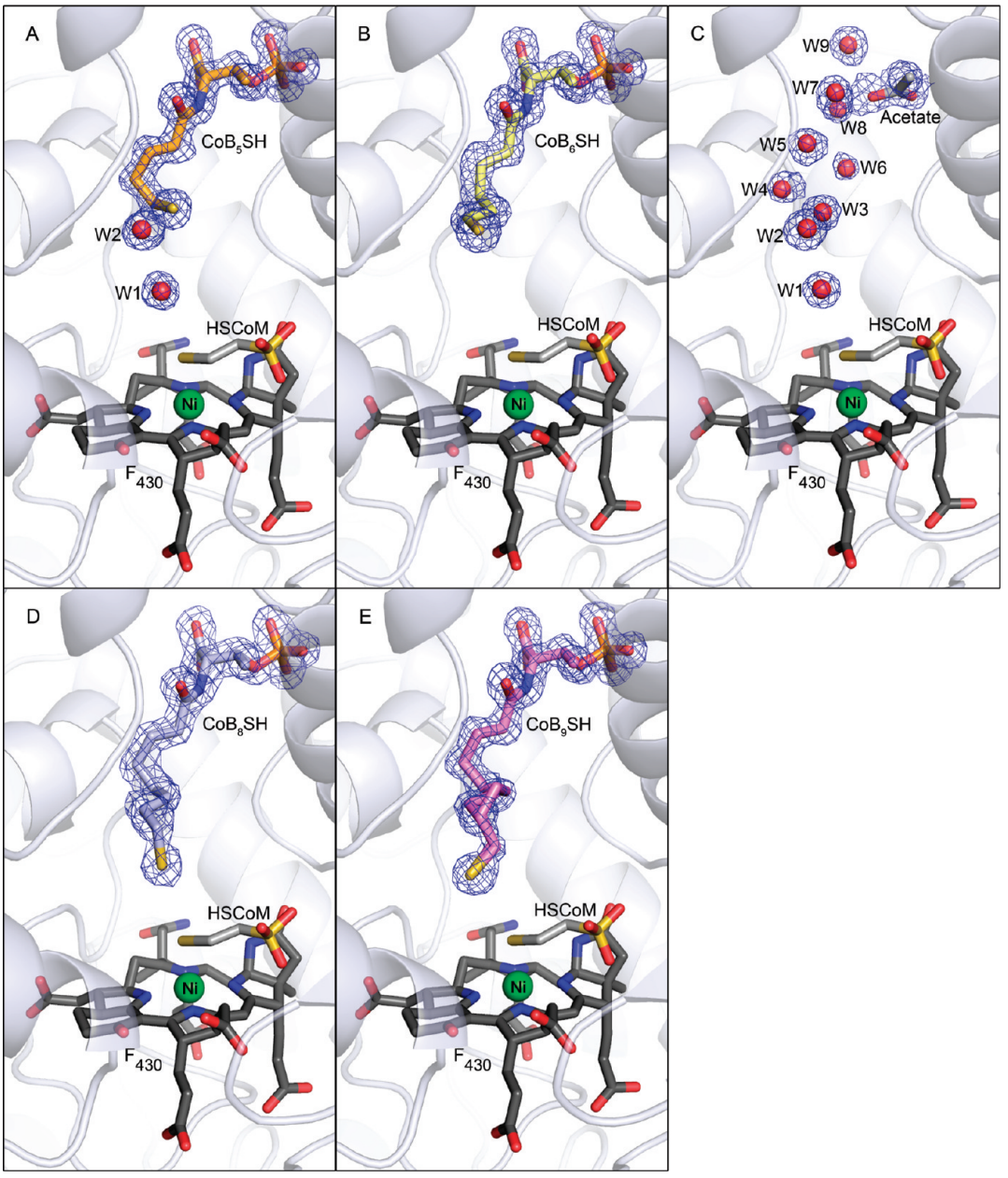

FIGURE 3: The active sites and substrate channels of the MCR crystal structures: (A) MCR_{CoB5SH}; (B) MCR_{CoB6SH}; (C) MCR_{HSCoM}; (D) MCR_{CoB8SH}; (E) MCR_{CoB9SH}. $2F_o - F_c$ electron density map around the CoB_XSH analogues; waters in the CoBSH binding part of the channel and the acetate ion (contoured at 1σ) are shown as a blue mesh. The protein is drawn as a cartoon. CoB_XSH and acetate are drawn as stick and colored by atom (carbon: CoB_5SH, orange; CoB_6SH, pale yellow; CoB_8SH, light blue; CoB_9SH, magenta; acetate, white). Coenzyme F_{430} and HSCoM are drawn as stick colored by atom (carbon: F_{430}, dark gray; HSCoM, medium gray). The nickel is displayed as a green sphere, and waters are displayed as red spheres. The figure was generated using PyMOL (http://www.pymol.org/).

absent sulfonate oxygen positions of HSCoM. Based on the presence of positive difference electron density, a third water was modeled ligated to the Ni and refined to a distance of ~2 Å (2.0 and 2.1 Å in the two active sites of the ASU) with no distance restraint imposed between the Ni and water. This water is in a similar position as the Ni coordinating sulfonate oxygen of the heterodisulfide product in MCR_{silent} (Supporting Information, Figure S6, and PDB codes 3m32 and 1hbm) (*5*, *33*). The fourth water was in the vicinity of the expected position of a bridging water (W1) seen in other structures (Figures 1 and 3A,C).

Water Structure in the Absence of CoBSH. The 1.45 Å resolution electron density obtained for MCR_{HSCoM} indicates that the substrate channel contains only 30% CoBSH. Nine ordered waters (W1−W9), along with an acetate ion from the crystallization solution, occupy the channel, with the acetate positioned where the phosphothreonine linkage of CoBSH would be (Figure 3C). Presumably one to two further waters would replace the acetate under physiological conditions. Other than W3 and W7, the waters form hydrogen bonds with protein (Figure 5). One water (W2) occupies the same site as the CoBSH thiol. Presumably due to the loss of favorable interactions that exist when CoBSH is present, the hydrophobic side chain of Valα482 adopts a second conformation modeled at 60% occupancy (Supporting Information, Figure S7).

Position of the "Bridging" Water, W1. The equivalent of W1 has previously been observed in $MCR_{red1\text{-}silent}$ and $MCR_{ox1\text{-}silent}$ crystal structures where, in the presence of CoBSH and HSCoM, it is sited equidistant (3.2 Å) between the two coenzyme thiols

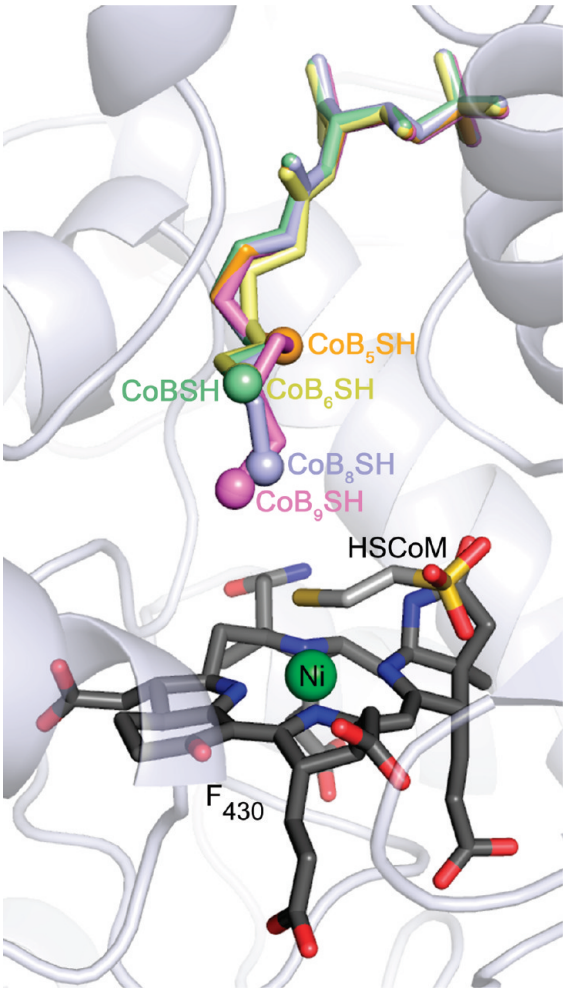

FIGURE 4: Overlay of CoBSH (from PDB code 1hbn) and the different CoBSH analogues. CoB$_X$SH are drawn as stick with the thiol represented by a sphere and colored as follows: CoB$_5$SH, orange; CoB$_6$SH, pale yellow; CoBSH, light green; CoB$_8$SH, light blue; CoB$_9$SH, magenta. The protein is drawn as a cartoon. Coenzyme F$_{430}$ and HSCoM are drawn as stick colored by atom (carbon: F$_{430}$, dark gray; HSCoM, medium gray). The nickel is displayed as a green sphere. The figure was generated using PyMOL (http://www.pymol.org/).

(PDB codes 1hbn, 1hbo, 1hbu) and thus been termed the "bridging water" (Figure 1) (*5*, *33*). However, in the MCR$_{HSCoM}$ structure, due to the presence of the more polarized W2 water, W1 is displaced away from HSCoM to maximize the hydrogen bond interaction with W2 (2.9 Å to W2; 3.5 Å to HSCoM thiol, Figure 5). In the MCR$_{CoB5SH}$ structure that also contained W2, the electron density indicated that this repositioning of W1 toward W2 also occurred. In contrast, the MCR$_{CoB6SH}$ structure contained 100% thiol at the CoBSH position but a partial occupancy of HSCoM (50%). In this case the electron density for W1 indicated it had moved toward the nickel to form an optimal hydrogen bond with a Ni-ligating water that was only present in the absence of HSCoM (3.7 Å to CoB$_{(6)}$SH thiol; 3.0 Å to Ni-ligating water, Supporting Information, Figure S5). In all structures reported here, W1 (if present) appears to be a sensitive indicator of the relative electronegativity of the Ni-ligated atom to that occupying the position of the CoBSH thiol and was a useful check in the crystallographic modeling and refinement process.

Flexibility in the Substrate Channel: Alternative Protein Conformers. The binding site of HSCoM (and presumably

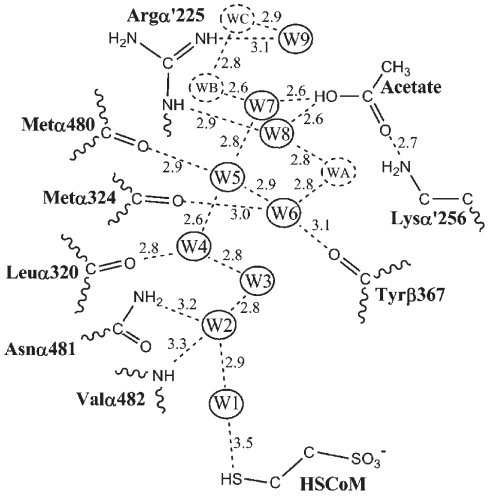

FIGURE 5: Hydrogen-bonding diagram for the water structure modeled in MCR$_{HSCoM}$. The water molecules are named as in Figure 3C (W1−W9); WA, WB, and WC are water molecules that are present in all structures (i.e., in concert with the substrate CoBSH and the CoBSH analogues). Interactions between surrounding residues and the water molecules are drawn as dashed lines, and the corresponding distance is indicated in angstroms (Å).

methyl-SCoM) is more deeply buried within the enzyme, and so it must enter prior to CoBSH for productive chemistry to occur. As binding of CoBSH in the absence of cosubstrate would be inhibitory, it was suggested that a conformational change upon methyl-SCoM binding might lower the K_d for CoBSH and thus promote an ordered mechanism. Compared to the 1hbn MCR$_{ox1\text{-}silent}$ and 1hbu MCR$_{red1c\text{-}silent}$ crystal structures, which both have full-occupancy HSCoM, the lower occupancy of HSCoM in the 1hbo MCR$_{red1\text{-}silent}$ structure was associated with significantly greater flexibility within the channel and the ability to model a second conformation of a Gly-rich amino acid stretch that formed part of the CoBSH channel. This suggested that methyl-SCoM binding might cause the channel to become more ordered, increasing the affinity of MCR for CoBSH by conformational restriction rather than a switch mechanism where the structure reorganizes from one well-defined conformer to another (*33*). In the MCR$_{HSCoM}$ data containing 30% CoBSH and 100% HSCoM, the $F_o - F_c$ difference electron density map at one of the two independent active sites in the ASU contained positive peaks that suggested the presence of an alternate conformation also involving this part of the polypeptide (Supporting Information, Figure S8). Using this as a guide, a similar second conformation involving seven contiguous amino acid residues of the same Gly-rich amino acid stretch (*β*366−372) could be modeled and refined at 20% occupancy leaving no residual difference density. Parts of the α′ subunit (α′111−129 and α′237−242) that are in close proximity to this stretch of amino acids also exhibit second conformations, with the main-chain carbonyl of α′243 in van der Waals contact with the B ring of F$_{430}$ tetrapyrrole (Supporting Information, Figure S9). Modeling these at 20% occupancy accounted for the weak positive $F_o - F_c$ difference electron density peaks observed in these areas. The evidence of alternate conformers in these areas lends support to the proposal that increased flexibility in the substrate channel propagates through the protein (*33*).

The MCR$_{CoB6SH}$ crystal structure contains 50% CoB$_6$SH, 50% CoBSH, and 50% HSCoM. In this case there is no evidence of an alternate loop conformation in either active site of the ASU.

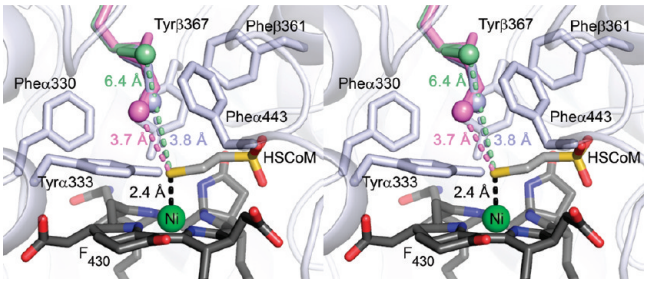

FIGURE 6: Stereo image of the annulus of aromatic amino acids proximal of coenzyme F_{430}. The protein is drawn as a cartoon with the side chains of the aromatic residues drawn as white stick. CoBSH (from PDB code 1hbn (*9*)), CoB_8SH, and CoB_9SH are drawn as stick with the thiols represented by spheres, and colored as follows: CoBSH, light green; CoB_8SH, light blue; CoB_9SH, magenta. Coenzyme F_{430} and HSCoM are drawn as stick colored by atom (carbon: F_{430}, dark gray; HSCoM, medium gray). The nickel is displayed as a green sphere. The figure was generated using PyMOL (http://www.pymol.org/).

However, as CoBSH and CoB_6SH combined are at 100% occupancy, it is not surprising their favorable interactions with the substrate channel would reduce conformational disorder, despite the partial occupancy of HSCoM.

Analogues Longer Than CoBSH: CoB_8SH and CoB_9SH. Both analogues could be accommodated in the MCR substrate channel (Figure 3D,E). The electron density supported final models containing 50% CoB_8SH for MCR_{CoB8SH} (1.8 Å resolution) and 60% CoB_9SH for MCR_{CoB9SH} (1.45 Å resolution). The phosphate headgroups are in identical positions to those of CoBSH, CoB_5SH, and CoB_6SH (Figure 4) (*5*, *33*). Both analogues follow the crystallographically observed chain path of bound CoBSH, with the extra atoms displacing the W1 water and placing the thiols closer to the nickel (Figure 6). CoB_9SH does have a second conformer that deviates from the CoBSH path, but the thiol position for this conformer and the CoBSH-tracking conformer are identical (Figure 3E and Supporting Information, Figure S10). Interestingly, the thiol of CoB_8SH is not coincident with the CoB_9SH carbon that precedes the CoB_9SH thiol (Figure 6). CoB_8SH is an MCR inhibitor with an apparent K_i of 15 μM (*3*). CoB_9SH has never been tested for inhibition of MCR-catalyzed methane formation, but it is reasonable to assume that it would be an inhibitor.

CoB_XSH Thiol-to-Nickel Spatial Relationship. The position of CoBSH in previous crystal structures poses a conundrum (*5*, *33*). In all the proposed catalytic mechanisms, CoBSH must interact with species generated at the nickel. Perplexingly, the sulfur of the CoBSH substrate is 8.8 Å from the Ni(II) in the $MCR_{ox1\text{-}silent}$ and both $MCR_{red1\text{-}silent}$ crystal structures and 6.4 Å from the thiol of the substrate analogue HSCoM (Figure 1). Modeling studies demonstrated that the addition of a methyl group to HSCoM did not bridge this gap (*35*, *45*, *53*). Therefore, a conformational change has been postulated that would enable CoBSH to penetrate deeper into the substrate channel and thus approach closer to any nickel-bound species. The heterodisulfide product in the MCR_{silent} crystal structure has the CoBSH portion in virtually the same place as in $MCR_{ox1\text{-}silent}$, giving no clue to possible structural changes that might occur to facilitate CoBSH reacting with nickel-associated intermediates (*5*, *33*).

Trigonometry suggests that if the alkanoyl chain of CoBSH or its analogue is in an extended conformation, each additional unit in the chain would lead to the thiol moving ~1.2 Å toward the Ni. Until this study there have been no crystal structures of CoBSH analogues in complex with MCR, so mechanistic studies using different chain length analogues of CoBSH assumed that shorter analogues would trace the observed path of CoBSH and longer analogues would penetrate about ~1.2 Å deeper per additional chain unit into the channel. In the case of the shortest analogue CoB_5SH, it does indeed follow the path of CoBSH, with the thiol of CoB_5SH being 2.8 Å away from the thiol position of CoBSH. However, due to the conformation CoBSH adopts when bound in the substrate channel, the difference in the S−Ni distance is small, the CoB_5SH thiol being only 0.5 Å farther from the Ni than CoBSH (8.8 Å for CoBSH vs 9.3 Å for CoB_5SH) (Table 2). This is due to the alkanoyl chain of CoBSH not being in an extended conformation from carbons 4 to 6 (carbon 1 is the carbonyl carbon). CoB_6SH, on the other hand, adopts a conformation that places its thiol in virtually the same position as the thiol of CoBSH (Figure 4 and Table 2). This is consistent with CoB_6SH being a substrate. However, the k_{cat} is 1000-fold lower than for CoBSH (*3*, *35*) although its K_m value (180 μM; Dey and Ragsdale, in preparation) is similar to that of CoBSH (K_m = 75 μM (*3*)). The reason for this may be that the shorter alkanoyl chain may not enable the analogue thiol to approach the nickel close enough for efficient catalysis and thus explain why CoB_6SH is such a poor substrate.

Table 2: Distances from Analogue Thiols

	CoB_XS−SCoM distance (Å)	CoB_XS−Ni distance (Å)
CoB_5SH	7.11/7.11[a]	9.30/9.30
CoB_6SH	6.26/6.26	8.70/8.70
CoB_7SH (substrate)[b]	6.37/6.39	8.73/8.77
CoB_8SH	3.75/3.78	6.16/6.17
CoB_9SH	3.71/3.68	5.96/5.91

[a]Distances in the two crystallographically independent active sites in the ASU. [b]Distances in the 1.16 Å resolution $MCR_{ox1\text{-}silent}$ structure (PDB code 1hbn) (*33*).

In the case of the longer CoB_XSH analogues, the sulfur of CoB_8SH is 2.6 Å closer to the Ni ion of F_{430} than that of CoBSH and 2.5 Å closer to the thiol of HSCoM (Figure 6 and Table 2). The CoB_9SH molecule follows the path of CoBSH and reaches only a little further into the substrate channel than CoB_8SH, with the CoB_9SH thiol positioned 2.9 Å closer to the Ni than the thiol of CoBSH (Figure 6 and Table 2). This is only 0.3 Å closer than the distance observed for the CoB_8SH thiol, even though they are noncoincident. The distance to the thiol of HSCoM is 2.6 Å closer than that of the substrate, CoBSH, only 0.1 Å closer than the CoB_8SH thiol. The two analogue thiols are above an annular hydrophobic aromatic environment created by Pheα330, Tyrα333, Pheα443, Pheβ361, and Tyrβ367 that lies between them and F_{430} (Figure 6). As a result, penetrating further into the channel may be energetically unfavorable, consistent with the small difference in relative distances between the CoB_8SH/CoB_9SH thiols and the HSCoM thiol/F_{430} nickel. The annulus is proposed to be catalytically important in positioning methyl-SCoM and stabilizing the methane product, and the tyrosines have been proposed to be proton donors associated with mechanism II (Scheme 2B) (*5*, *33*).

Thus, there appear to be three preferential distances for thiols (including that of HSCoM) within the MCR substrate channel: CoB_6SH/CoBSH at 8.7−8.8 Å, CoB_8SH/CoB_9SH at 5.9−6.2 Å, and HSCoM at 2.4 Å from the nickel of F_{430} (Table 2).

Recent ENDOR, high-field continuous and pulse EPR work has identified changes in nickel coordination when CoBSH

is added to MCR_{red1c} (active Ni(I)-MCR_{red1} + HSCoM) (*14*, *15*, *18*, *31*). This generates up to 50% MCR_{red2} which is comprised of two distinct nickel coordination geometries: an axial MCR_{red2a} formally assigned as a Ni(III)-hydride and a rhombic MCR_{red2r} in which the thiol of HSCoM is a Ni(I) ligand (Supporting Information, Scheme S1). Formation of MCR_{red2} could also be induced by addition of CoBSH substrate analogues CoBS-CH_3 and CoBS-CF_3, which have a chain length one unit longer than substrate CoBSH (*18*, *53*). The CoBS-CF_3 enabled ^{19}F-ENDOR studies to be performed and demonstrated that following CoBS-CF_3 addition the remaining MCR_{red1} species had Ni(I)$-^{19}F$ distances of 6.2−7.7 Å. This distance range agreed with a CoBS-CF_3 model created using the CoBSH position observed in the $MCR_{ox1\text{-}silent}$ crystal structure (*53*). However, in the MCR_{red2} species the Ni(I)$-^{19}F$ distances had shortened, indicating a movement of ~2 Å toward the nickel (MCR_{red2a} Ni(I)$-^{19}F$, 4.0−5.5 Å; MCR_{red2r} Ni(I)$-^{19}F$, 4.5−5.7 Å). In the case of the CoB_8SH analogue (the closest equivalent to CoBS-CF_3 used in this study) the thiol to Ni(II) distance lies between the distance ranges observed in the CoBS-CF_3 studies, and so the fluorine(s) of the CoBS-CF_3 in MCR_{red2} might penetrate a little further into the hydrophobic annulus in the MCR_{red2} species. As the alkanoyl chain of CoBSH is not fully extended, it could easily undergo a similar conformation change to that observed in the MCR_{red2} state.

Reaction of MCR Ni(III)-Alkyl Species with CoB_8SH and CoB_9SH. The two longer CoB_XSH analogues have been shown to undergo alkylation when reacted with MCR_{PS}, a [Ni(III)-propyl ↔ Ni(II)-propylsulfonate radical] formed from reaction of Ni(I)-MCR_{red1} with bromopropanesulfonate (BPS) (Supporting Information, Scheme S1) (*20*, *23*, *30*, *45*, *54*). BPS is a substrate of MCR_{red1} in a reaction that involves a rapid CoBSH-independent nucleophilic attack by Ni(I) on BPS to displace bromide and generate MCR_{PS} at a rate ~60-fold faster than generation of methane from CoBSH and methyl-HSCoM (*20*, *45*). Certain thiols can eliminate the propylsulfonate to yield a thioether product and regenerate MCR_{red1}, although at a rate 1000-fold slower than methane formation (*45*). Both CoB_8SH and CoB_9SH can react with MCR_{PS} to regenerate MCR_{red1}, but CoBSH cannot. The overall second-order rate constant for the reactivation of MCR by CoB_8SH is 160 M^{-1} s^{-1}, whereas for CoB_9SH the reaction is more sluggish (12 M^{-1} s^{-1}). CoB_9SH might be expected to be closer to the proximal Ni ligand. It was therefore proposed that this caused steric interference and explained why CoB_9SH was a poorer reactivator of MCR than CoB_8SH. Our study has shown that the thiols of these two analogues are placed such that they are approximately the same distance (~3.7 Å) from the thiol of HSCoM ligated to the Ni atom (Table 2). The Ni(II)−HSCoM bond is 2.4 Å, whereas an Ni(III)−alkyl bond is expected to be ~2 Å (*24*, *33*), indicating that a conformational change is required to effect the nucleophilic attack of the CoB_8SH and CoB_9SH thiols on an alkyl-bound species. It would appear that a conformational change, such as observed in MCR_{red2}, is required for this chemistry also (*53*).

A Ni(III)-alkyl species is akin to the first intermediate in mechanism I of MCR-catalyzed methane formation, Ni(III)-methyl (MCR_{Me}, Supporting Information, Scheme S1, Scheme 2A) (*11*, *27*). MCR_{Me} has been shown to be capable of generating MCR_{red1} and methyl-SCoM upon addition of HSCoM (which is the reverse of mechanism I, step 1, Scheme 2A), similar chemistry to the observed formation of a thioether product from the Ni(III)-alkyl. Further addition of CoBSH following HSCoM treatment of MCR_{Me} led to methane and heterodisulfide formation, the natural products of methanogenesis. Although this lends credence to mechanism I, it should be noted that, like MCR_{PS}, MCR_{Me} in these experiments was generated artificially. The MCR_{CoB9SH} crystal structure demonstrates that the two additional methylene units in the alkanoyl chain, cf. CoBSH, do not necessarily translate into direct interaction of the thiol with the nickel proximal ligand. However, this could represent the favorable position for a CoBSH thiol interacting with the methyl group of methyl-SCoM. Just as the alkanoyl chain of CoB_6SH has a more extended conformation than CoBSH in the substrate channel, CoBSH could also adopt a more extended conformation so that its thiol was in a similar position as the thiol of CoB_8SH, priming it for reaction with a nickel-bound species.

If a significant conformational change is required early in MCR-catalyzed chemistry, which would be a requirement of mechanism I, catalysis may well involve a rearrangement of the aromatic amino acid annulus due to the presence of the methyl of methyl-SCoM, and this might enable deeper penetration of CoBSH into MCR (Figure 6). All of the crystal structures in this study, and those solved previously, are of the inactive Ni(II)-MCR, which appears to disfavor close approach to the nickel in the absence of Ni(I)-bound methyl-SCoM, even in the case of CoB_9SH.

CONCLUSION

The goal of this study was to induce structural changes within the substrate channel and active site of MCR using analogues of coenzyme CoBSH. It was hoped that this would shed light on the nature of conformational changes that have been proposed to occur in MCR catalysis. We have shown that the CoB_XSH analogues do not lead to any significant conformational changes within the context of inactive Ni(II)-MCR. Therefore, it may be that methyl-SCoM is the key coenzyme, in combination with a nickel oxidation state of +1 (and +3), that triggers a conformational change bringing the thiol of CoBSH closer to the nickel. Thus, the crystal structure of the Ni(I)-methyl-SCoM/MCR complex may be the key to structurally define conformational changes required for MCR-mediated chemistry.

ACKNOWLEDGMENT

X-ray data were collected at beamline 14-BM-C and photoreduction studies at 14-ID-B, BioCARS, at the Advanced Photon Source (APS), Argonne National Laboratory, Argonne, IL. We thank Vukica Srajer and Yu-Sheng Chen for valuable assistance during data collection. Use of the Advanced Photon Source was supported by the U.S. Department of Energy, Basic Energy Sciences, Office of Science under Contract DE-AC02-06CH11357. Use of the BioCARS Sector 14 was supported by the National Institutes of Health, National Center for Research Resources, under Grant RR007707. Computer resources were provided by the Basic Sciences Computing Laboratory of the University of Minnesota Supercomputing Institute, and we thank Can Ergenekan for support. We also thank Ed Hoeffner at the Kahlert Structural Biology Laboratory (KSBL) at the University of Minnesota. Use of the KSBL was supported by Minnesota Partnership for Biotechnology and Medical Genomics Grant SPAP-05-0013-P-FY06.

SUPPORTING INFORMATION AVAILABLE

Material and methods for single crystal UV−visible microspectrophotometry, X-ray photoreduction experiment, and X-ray

crystallography of the MCR−heterodisulfide product complex ($MCR_{CoBSH+methyl\text{-}SCoM}$); results and discussion for redox changes and $MCR_{CoBSH+methyl\text{-}SCoM}$ crystal structure; Table S1, X-ray data collection, processing and refinement statistics for $MCR_{CoBSH+methyl\text{-}SCoM}$; Figure S1, use of $F_o - F_c$ electron density in modeling MCR_{CoB8SH}; Figure S2, illustration of electron density quality of MCR_{CoB5SH}; Figure S3, solution and single crystal UV−visible spectra; Figure S4, modeling of CoB_6SH and CoBSH into the electron density of MCR_{CoB6SH}; Figure S5, partially occupied HSCoM in MCR_{CoB6SH}; Figure S6, the active site and substrate channel of $MCR_{CoBSH+methyl\text{-}SCoM}$; Figure S7, alternative conformation of Valα482 in MCR_{HSCoM}; Figure S8, the two conformations of the Gly-rich loop in MCR_{HSCoM}; Figure S9, propagation of conformational changes in MCR_{HSCoM}; Figure S10, the two conformations of CoB_9SH in MCR_{CoB9SH}; Figure S11, EPR spectra of MCR_{red1} sample; Scheme S1, scheme of the characterized forms of MCR. This material is available free of charge via the Internet at http://pubs.acs.org.

REFERENCES

1. Thauer, R. K. (1998) Biochemistry of methanogenesis: a tribute to Marjory Stephenson. *Microbiology 144*, 2377–2406.
2. Thauer, R. K., and Shima, S. (2008) Methane as fuel for anaerobic microorganisms. *Ann. N.Y. Acad. Sci. 1125*, 158–170.
3. Ellermann, J., Hedderich, R., Bocher, R., and Thauer, R. K. (1988) The final step in methane formation. Investigations with highly purified methyl-CoM reductase (component C) from *Methanobacterium thermoautotrophicum* (strain Marburg). *Eur. J. Biochem. 172*, 669–677.
4. Ellefson, W. L., and Wolfe, R. S. (1981) Component C of the methylreductase system of *Methanobacterium*. *J. Biol. Chem. 256*, 4259–4262.
5. Ermler, U., Grabarse, W., Shima, S., Goubeaud, M., and Thauer, R. K. (1997) Crystal structure of methyl-coenzyme M reductase: the key enzyme of biological methane formation. *Science 278*, 1457–1462.
6. Diekert, G., Gilles, H. H., Jaenchen, R., and Thauer, R. K. (1980) Incorporation of 8 succinate per mol nickel into factors F430 by *Methanobacterium thermoautotrophicum*. *Arch. Microbiol. 128*, 256–262.
7. Diekert, G., Jaenchen, R., and Thauer, R. K. (1980) Biosynthetic evidence for a nickel tetrapyrrole structure of factor F_{430} from *Methanobacterium thermoautotrophicum*. *FEBS Lett. 119*, 118–120.
8. Whitman, W. B., and Wolfe, R. S. (1980) Presence of nickel in factor F430 from *Methanobacterium bryantii*. *Biochem. Biophys. Res. Commun. 92*, 1196–1201.
9. Albracht, S. P. J., Ankel-Fuchs, D., Böcher, R., Ellermann, J., Moll, J., van der Zwann, J. W., and Thauer, R. K. (1988) Five new EPR signals assigned to nickel in methyl-coenzyme M reductase from *Methanobacterium thermoautotrophicum*, strain Marburg. *Biochim. Biophys. Acta 955*, 86–102.
10. Dey, M., Kunz, R. C., Lyons, D. M., and Ragsdale, S. W. (2007) Characterization of alkyl-nickel adducts generated by reaction of methyl-coenzyme m reductase with brominated acids. *Biochemistry 46*, 11969–11978.
11. Dey, M., Telser, J., Kunz, R. C., Lees, N. S., Ragsdale, S. W., and Hoffman, B. M. (2007) Biochemical and spectroscopic studies of the electronic structure and reactivity of a methyl-Ni species formed on methyl-coenzyme M reductase. *J. Am. Chem. Soc. 129*, 11030–11032.
12. Duin, E. C., Cosper, N. J., Mahlert, F., Thauer, R. K., and Scott, R. A. (2003) Coordination and geometry of the nickel atom in active methyl-coenzyme M reductase from *Methanothermobacter marburgensis* as detected by X-ray absorption spectroscopy. *J. Biol. Inorg. Chem. 8*, 141–148.
13. Duin, E. C., Signor, L., Piskorski, R., Mahlert, F., Clay, M. D., Goenrich, M., Thauer, R. K., Jaun, B., and Johnson, M. K. (2004) Spectroscopic investigation of the nickel-containing porphinoid cofactor F(430). Comparison of the free cofactor in the (+)1, (+)2 and (+)3 oxidation states with the cofactor bound to methyl-coenzyme M reductase in the silent, red and ox forms. *J. Biol. Inorg. Chem. 9*, 563–576.
14. Finazzo, C., Harmer, J., Bauer, C., Jaun, B., Duin, E. C., Mahlert, F., Goenrich, M., Thauer, R. K., Van Doorslaer, S., and Schweiger, A. (2003) Coenzyme B induced coordination of coenzyme M via its thiol group to Ni(I) of F430 in active methyl-coenzyme M reductase. *J. Am. Chem. Soc. 125*, 4988–4989.
15. Finazzo, C., Harmer, J., Jaun, B., Duin, E. C., Mahlert, F., Thauer, R. K., Van Doorslaer, S., and Schweiger, A. (2003) Characterization of the MCRred2 form of methyl-coenzyme M reductase: a pulse EPR and ENDOR study. *J. Biol. Inorg. Chem. 8*, 586–593.
16. Goubeaud, M., Schreiner, G., and Thauer, R. K. (1997) Purified methyl-coenzyme-M reductase is activated when the enzyme-bound coenzyme F430 is reduced to the nickel(I) oxidation state by titanium(III) citrate. *Eur. J. Biochem. 243*, 110–114.
17. Harmer, J., Finazzo, C., Piskorski, R., Bauer, C., Jaun, B., Duin, E. C., Goenrich, M., Thauer, R. K., Van Doorslaer, S., and Schweiger, A. (2005) Spin density and coenzyme M coordination geometry of the ox1 form of methyl-coenzyme M reductase: a pulse EPR study. *J. Am. Chem. Soc. 127*, 17744–17755.
18. Harmer, J., Finazzo, C., Piskorski, R., Ebner, S., Duin, E. C., Goenrich, M., Thauer, R. K., Reiher, M., Schweiger, A., Hinderberger, D., and Jaun, B. (2008) A nickel hydride complex in the active site of methyl-coenzyme m reductase: implications for the catalytic cycle. *J. Am. Chem. Soc. 130*, 10907–10920.
19. Hinderberger, D., Ebner, S., Mayr, S., Jaun, B., Reiher, M., Goenrich, M., Thauer, R. K., and Harmer, J. (2008) Coordination and binding geometry of methyl-coenzyme M in the red1m state of methyl-coenzyme M reductase. *J. Biol. Inorg. Chem. 13*, 1275–1289.
20. Kunz, R. C., Horng, Y. C., and Ragsdale, S. W. (2006) Spectroscopic and kinetic studies of the reaction of bromopropanesulfonate with methyl-coenzyme M reductase. *J. Biol. Chem. 281*, 34663–34676.
21. Mahlert, F., Bauer, C., Jaun, B., Thauer, R. K., and Duin, E. C. (2002) The nickel enzyme methyl-coenzyme M reductase from methanogenic archaea: in vitro induction of the nickel-based MCR-ox EPR signals from MCR-red2. *J. Biol. Inorg. Chem. 7*, 500–513.
22. Mahlert, F., Grabarse, W., Kahnt, J., Thauer, R. K., and Duin, E. C. (2002) The nickel enzyme methyl-coenzyme M reductase from methanogenic archaea: in vitro interconversions among the EPR detectable MCR-red1 and MCR-red2 states. *J. Biol. Inorg. Chem. 7*, 101–112.
23. Rospert, S., Voges, M., Berkessel, A., Albracht, S. P., and Thauer, R. K. (1992) Substrate-analogue-induced changes in the nickel-EPR spectrum of active methyl-coenzyme-M reductase from *Methanobacterium thermoautotrophicum*. *Eur. J. Biochem. 210*, 101–107.
24. Sarangi, R., Dey, M., and Ragsdale, S. W. (2009) Geometric and electronic structures of the Ni(I) and methyl-Ni(III) intermediates of methyl-coenzyme M reductase. *Biochemistry 48*, 3146–3156.
25. Tang, Q., Carrington, P. E., Horng, Y. C., Maroney, M. J., Ragsdale, S. W., and Bocian, D. F. (2002) X-ray absorption and resonance Raman studies of methyl-coenzyme M reductase indicating that ligand exchange and macrocycle reduction accompany reductive activation. *J. Am. Chem. Soc. 124*, 13242–13256.
26. Telser, J., Davydov, R., Horng, Y. C., Ragsdale, S. W., and Hoffman, B. M. (2001) Cryoreduction of methyl-coenzyme M reductase: EPR characterization of forms, MCR(ox1) and MCR (red1). *J. Am. Chem. Soc. 123*, 5853–5860.
27. Yang, N., Reiher, M., Wang, M., Harmer, J., and Duin, E. C. (2007) Formation of a nickel-methyl species in methyl-coenzyme M reductase, an enzyme catalyzing methane formation. *J. Am. Chem. Soc. 129*, 11028–11029.
28. Albracht, S. P. J., Ankelfuchs, D., Vanderzwaan, J. W., Fontijn, R. D., and Thauer, R. K. (1986) A new electron-paramagnetic-res signal of nickel in *Methanobacterium thermoautotrophicum*. *Biochim. Biophys. Acta 870*, 50–57.
29. Telser, J., Horng, Y. C., Becker, D. F., Hoffman, B. M., and Ragsdale, S. W. (2000) On the assignment of nickel oxidation states of the Ox1, Ox2 forms of methyl-coenzyme M reductase. *J. Am. Chem. Soc. 122*, 182–183.
30. Hinderberger, D., Piskorski, R. R., Goenrich, M., Thauer, R. K., Schweiger, A., Harmer, J., and Jaun, B. (2006) A nickel-alkyl bond in an inactivated state of the enzyme catalyzing methane formation. *Angew. Chem., Int. Ed. 45*, 3602–3607.
31. Kern, D. I., Goenrich, M., Jaun, B., Thauer, R. K., Harmer, J., and Hinderberger, D. (2007) Two sub-states of the red2 state of methyl-coenzyme M reductase revealed by high-field EPR spectroscopy. *J. Biol. Inorg. Chem. 12*, 1097–1105.
32. Becker, D. F., and Ragsdale, S. W. (1998) Activation of methyl-SCoM reductase to high specific activity after treatment of whole cells with sodium sulfide. *Biochemistry 37*, 2639–2647.
33. Grabarse, W., Mahlert, F., Duin, E. C., Goubeaud, M., Shima, S., Thauer, R. K., Lamzin, V., and Ermler, U. (2001) On the mechanism of biological methane formation: structural evidence for conformational changes in methyl-coenzyme M reductase upon substrate binding. *J. Mol. Biol. 309*, 315–330.

34. Grabarse, W., Mahlert, F., Shima, S., Thauer, R. K., and Ermler, U. (2000) Comparison of three methyl-coenzyme M reductases from phylogenetically distant organisms: unusual amino acid modification, conservation and adaptation. *J. Mol. Biol. 303*, 329–344.
35. Horng, Y. C., Becker, D. F., and Ragsdale, S. W. (2001) Mechanistic studies of methane biogenesis by methyl-coenzyme M reductase: evidence that coenzyme B participates in cleaving the C-S bond of methyl-coenzyme M. *Biochemistry 40*, 12875–12885.
36. Berkessel, A. (1991) Methyl-coenzyme-M reductase—Model studies on pentadentate nickel-complexes and a hypothetical mechanism. *Bioorg. Chem. 19*, 101–115.
37. Jaun, B. (1990) Coenzyme-F430 from methanogenic bacteria—Oxidation of F430 pentamethyl ester to the Ni(III) form. *Helv. Chim. Acta 73*, 2209–2217.
38. Signor, L., Knuppe, C., Hug, R., Schweizer, B., Pfaltz, A., and Jaun, B. (2000) Methane formation by reaction of a methyl thioether with a photo-excited nickel thiolate—A process mimicking methanogenesis in archaea. *Chem.—Eur. J. 6*, 3508–3516.
39. Chen, S. L., Pelmenschikov, V., Blomberg, M. R., and Siegbahn, P. E. (2009) Is there a Ni-methyl intermediate in the mechanism of methyl-coenzyme M reductase? *J. Am. Chem. Soc. 131*, 9912–9913.
40. Pelmenschikov, V., Blomberg, M. R. A., Siegbahn, P. E. M., and Crabtree, R. H. (2002) A mechanism from quantum chemical studies for methane formation in methanogenesis. *J. Am. Chem. Soc. 124*, 4039–4049.
41. Pelmenschikov, V., and Siegbahn, P. E. (2003) Catalysis by methyl-coenzyme M reductase: a theoretical study for heterodisulfide product formation. *J. Biol. Inorg. Chem. 8*, 653–662.
42. Duin, E. C., and McKee, M. L. (2008) A new mechanism for methane production from methyl-coenzyme M reductase as derived from density functional calculations. *J. Phys. Chem. B 112*, 2466–2482.
43. Bobik, T. A., and Wolfe, R. S. (1988) Physiological importance of the heterodisulfide of coenzyme M and 7-mercaptoheptanoylthreonine phosphate in the reduction of carbon dioxide to methane in *Methanobacterium*. *Proc. Natl. Acad. Sci. U.S.A. 85*, 60–63.
44. Goenrich, M., Duin, E. C., Mahlert, F., and Thauer, R. K. (2005) Temperature dependence of methyl-coenzyme M reductase activity and of the formation of the methyl-coenzyme M reductase red2 state induced by coenzyme B. *J. Biol. Inorg. Chem. 10*, 333–342.
45. Kunz, R. C., Dey, M., and Ragsdale, S. W. (2008) Characterization of the thioether product formed from the thiolytic cleavage of the alkyl-nickel bond in methyl-coenzyme M reductase. *Biochemistry 47*, 2661–2667.
46. Noll, K. M., Donnelly, M. I., and Wolfe, R. S. (1987) Synthesis of 7-mercaptoheptanoylthreonine phosphate and its activity in the methylcoenzyme M methylreductase system. *J. Biol. Chem. 262*, 513–515.
47. Olson, K. D., McMahon, C. W., and Wolfe, R. S. (1991) Photoactivation of the 2-(methylthio)ethanesulfonic acid reductase from *Methanobacterium*. *Proc. Natl. Acad. Sci. U.S.A. 88*, 4099–4103.
48. Zehnder, A. J., and Wuhrmann, K. (1976) Titanium(III) citrate as a nontoxic oxidation-reduction buffering system for the culture of obligate anaerobes. *Science 194*, 1165–1166.
49. Gunsalus, R. P., Romesser, J. A., and Wolfe, R. S. (1978) Preparation of coenzyme M analogues and their activity in the methyl coenzyme M reductase system of *Methanobacterium thermoautotrophicum*. *Biochemistry 17*, 2374–2377.
50. Otwinowski, Z., and Minor, W. (1997) Processing of X-ray diffraction data collected in oscillation mode. *Methods Enzymol.: Macromol. Crystallogr., Part A 276*, 307–326.
51. (1994) The CCP4 suite: programs for protein crystallography, *Acta Crystallogr., Sect. D: Biol. Crystallogr.* 50, 760-763.
52. Emsley, P., and Cowtan, K. (2004) Coot: model-building tools for molecular graphics. *Acta Crystallogr., Sect. D: Biol. Crystallogr. 60*, 2126–2132.
53. Ebner, S., Jaun, B., Goenrich, M., Thauer, R. K., and Harmer, J. (2010) Binding of coenzyme B induces a major conformational change in the active site of methyl-coenzyme M reductase. *J. Am. Chem. Soc. 132*, 567–575.
54. Goenrich, M., Mahlert, F., Duin, E. C., Bauer, C., Jaun, B., and Thauer, R. K. (2004) Probing the reactivity of Ni in the active site of methyl-coenzyme M reductase with substrate analogues. *J. Biol. Inorg. Chem. 9*, 691–705.